metals

MDPI

Article

Effect of Deep Cryogenic Time on the Microstructure and Mechanical Property of Cr-Mn-Si High-Strength Alloy Steel

Jingyu Zhang [1,2,*], Haian Mao [1], Yi Meng [3,*], Rong Shi [3] and Jiamin Fang [3]

[1] School of Material Science and Engineering, Lanzhou University of Technology, Lanzhou 730050, China
[2] State Key Laboratory of Advanced Processing and Recycling of Non-Ferrous Metals, Lanzhou University of Technology, Lanzhou 730050, China
[3] College of Materials Science and Engineering, Chongqing University, Chongqing 400044, China; fangjm_cqu@163.com (J.F.)
* Correspondence: zhangjy@lut.edu.cn (J.Z.); mengyi@cqu.edu.cn (Y.M.); Tel.: +86-18794216276 (J.Z.)

Abstract: Cr-Mn-Si alloyed high-strength steel was subjected to deep cryogenic treatment after quenching and tempering (Q-T), and the microstructure and property evolution of the alloy steel after deep cryogenic treatment were studied. The tensile strength increased by about 30 MPa, the yield strength decreased by about 10 MPa, and the grains of alloy steel were refined, indicating that the strength and toughness of the alloy steel can be relatively improved via the deep cryogenic treatment (−120 °C × 1 h); the secondary carbides precipitated inside the martensitic matrix were uniformly distributed; and the average size was also significantly reduced, presenting a more uniform microstructure than that of the Q-T samples. Furthermore, the dislocation density of alloy steel also evolved during the deep cryogenic treatment, with the highest dislocation density after the 2 h treatment, thus providing a dislocation-strengthening effect. Therefore, the overall properties of the alloyed steel could be comprehensively improved by the deep cryogenic treatment after Q-T.

Keywords: Cr-Mn-Si-alloyed high-strength steel; deep cryogenic treatment; dislocation density; microstructure property

Citation: Zhang, J.; Mao, H.; Meng, Y.; Shi, R.; Fang, J. Effect of Deep Cryogenic Time on the Microstructure and Mechanical Property of Cr-Mn-Si High-Strength Alloy Steel. *Metals* **2023**, *13*, 1449. https://doi.org/10.3390/met13081449

Academic Editor: Hannu Hänninen

Received: 30 June 2023
Revised: 6 August 2023
Accepted: 9 August 2023
Published: 11 August 2023

1. Introduction

Cr-Mn-Si-alloyed steel is a series of low-alloy high-strength structural steels with ultra-high strength, good plastic toughness, and fatigue resistance that are mainly used for stressed parts manufacturing, such as aircraft beams, landing gear, wings, engine shafts, high-strength bolts, and solid rocket motor cases [1–5]. The performance requirements for the manufacturing materials are also increased due to the severe requirements of their working environment on the quality of the mold. Improving the mechanical properties of Cr-Mn-Si-alloyed high-strength steel by methods such as a heat treatment process have been utilized. Duan et al. [6] studied the effect of Ni addition on 30CrMnSiNi2A steel using the hot isostatic pressing technique, and the results showed that the matrix structure of C and Ni atoms were solid-solution-strengthened with the increase in Ni addition, and that the hardenability and tensile strength of 30CrMnSiNi2A steel were effectively improved. Dwivedi et al. [7] studied the effect of laser impact strengthening on the fatigue life of HSLA steel, and the results showed that laser impact strengthening significantly improved the mechanical properties of the surface, but that the surface roughness was not significantly reduced, which significantly reduced the strain mechanism, thus prolonging the fatigue life. Yuan et al. [8] conducted an experimental study on the mechanical properties of three kinds of 30CrMnSiNi2A steels with different carbon content at different tempering temperatures, and analyzed their microstructure and fracture morphology. Zhou et al. [9] investigated the effect of heat treatment on the microstructure and dynamic properties of 30CrMnSiNi2A steel, and the results showed that the yield strength of the steel increased with strain rate after different heat treatments, and that, by subjecting the steel material to the conventional

quenching–tempering heat treatment process, the hardness, yield strength, tensile strength, elongation, and impact toughness can be greatly improved, and better overall mechanical properties can be obtained. However, for some high-strength special workpieces, it is necessary to further refine the grain size to improve the mechanical properties of the steel materials, so some new heat treatment processes should be added based on the quenching and tempering process.

Deep cryogenic treatment is a kind of ultra-low-temperature treatment: a process of heat treatment of materials under a low-temperature environment (usually below −100 °C) [10–13] with liquid nitrogen as the refrigerant. Deep cryogenic treatment technology not only has the characteristics of a low cost, low energy consumption, no damage to the workpiece, and no pollution, but also plays a role in stabilizing the dimensions, improving the uniformity, reducing the deformation, etc. [14], so it has attracted much attention and has a broad range of market application. Hu et al. [15] studied the effect of the deep cryogenic treatment process on the microstructure and properties of M2 HSS and found that the microstructure transformation of residual austenite to martensite was promoted, resulting in irreversible changes in the microstructure of the material to varying degrees; thus, the strength, hardness, and toughness of the material were increased. Wang et al. [16] studied the effect of the number of deep cryogenic treatments on the wear property and corrosion resistance of E690 steel, and the results showed that the deep cryogenic treatment promoted the transformation of the microstructure to martensite and bainite of the specimen, and that fine carbides precipitated and diffused in the matrix, thus improving the wear resistance, corrosion resistance, and fatigue resistance of E690 steel. Li et al. [17] studied the effect of deep cryogenic time on the properties of GCr15-bearing steel and found that the residual austenite content decreased and the strength and wear resistance of the steel increased significantly with the extension of deep cryogenic time. Zhao et al. [18] tested Inconel 617 alloy by deep cryogenic treatment under different treatment times and the number of times, and the results showed that the grain size of Inconel 617 alloy was refined after deep cryogenic treatment, and that the fraction of small angle grain boundaries of the alloy increased, which contributed to the improvement in the tensile strength and plasticity of the alloy. Jurci et al. [19] studied the effect of deep cryogenic treatment and tempering on the corrosion behavior of Vanadis6 HSS steel and found that a subzero treatment of Vanadis6 steel significantly reduced the residual austenite content, refined the martensite, enhanced the carbide density, and changed the precipitation behavior, effectively suppressing the corrosion rate. Perez et al. [20] investigated the mechanical properties of AISI H13 steel by low-temperature treatment. The results showed that a deep cryogenic treatment of H13 steel induced higher thermal stresses and structural defects, and that tempering resulted in a dispersed network of fine carbides, which significantly improved the fracture toughness of the steel without altering other mechanical properties. The effect of the quenching–tempering process + deep cryogenic treatment on the mechanical properties of steel has also been studied. Dhokey et al. [21] investigated the effect of different tempering temperatures (200 °C, 300 °C, 400 °C) on H13 tool steel after deep cryogenic treatment, and the experimental results showed that a higher wear resistance was obtained after tempering at 200 °C due to the higher nucleation rate of tertiary carbides. Otherwise, by the continued processing of the deep cryogenic treatment on GCr15-bearing steel treated by quenching–tempering heat treatment, the residual austenite content in the specimen was significantly reduced compared with the conventional quenching–tempering heat treatment [22] because of the phase transformation and microstructure decomposition of the residual austenite martensitic during the deep cryogenic treatment, while the precipitation of small and diffused carbides in the subsequent tempering process was promoted, and the comprehensive mechanical properties of steel materials were further improved. The research on the quenching and tempering process + deep cryogenic treatment have mainly been focused on high-temperature alloys and amorphous alloys, but studies are relatively rare regarding the low-temperature properties of Cr-Mn-Si-alloyed high-strength steel.

The effect of the quenching and tempering process (Q-T process) + deep cryogenic process on the microstructure and properties of Cr-Mn-Si-alloyed high-strength steel is still

unclear; therefore, this study will add the deep cryogenic process after the conventional heat treatment process to deal with Cr-Mn-Si-alloyed high-strength steel, and will compare the effect of the deep cryogenic process time on the microstructure and mechanical properties of Cr-Mn-Si-alloyed high-strength steel, aiming to further improve the comprehensive properties of Cr-Mn-Si-alloyed high-strength steel and provide a reference for optimizing the deep cryogenic process.

2. Experimental Procedure

2.1. Initial Material

A Cr-Mn-Si-alloyed high-strength steel prepared by hot forging and annealing treatment was selected in this study. The initial microstructure is shown in Figure 1, and the grains were all non-directional equiaxed crystals with an average grain size of 16.6 μm. The chemical composition of the Cr-Mn-Si-alloyed high-strength steel is listed in Table 1. The total amount of alloying elements was not higher than 5%, and the added alloying elements were mainly used to improve the hardenability of the steel, increase the tempering, and improve the mechanical properties.

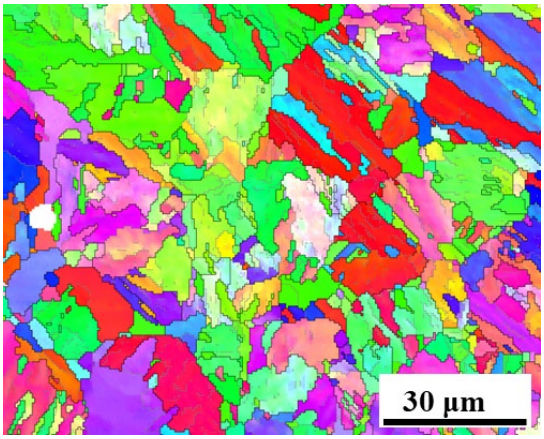

Figure 1. The initial microstructure of Cr-Mn-Si-alloyed high-strength steel.

Table 1. Chemical composition of Cr-Mn-Si-alloyed high-strength steel (wt.%).

C	Si	Mn	Cr	Mo	Ni	Al	S	Cu	Fe
0.285	0.992	1.120	1.090	0.006	2.040	0.011	0.033	0.218	Bal

2.2. Heat Treatment

The Q-T process was utilized for Cr-Mn-Si-alloyed high-strength steel to ensure the high residual austenite content. Combining the process with phase transformation strengthening and fine grain strengthening, a match of high strength and good plasticity was obtained and the comprehensive mechanical properties of the material could be effectively improved. For Cr-Mn-Si-alloyed high-strength steel, the use of deep cryogenic treatment technology after the Q-T process could further improve the ratio of various microstructure and comprehensive mechanical properties. This paper attempted to find relatively better process parameters of deep cryogenic process to improve its strength under the premise of ensuring a smaller reduction in plasticity so that the comprehensive mechanical properties can be further improved based on the Q-T process.

The experimental scheme of the Q-T + deep cryogenic process adopted in the paper is as follows: the alloy steel samples were heated for austenitizing (900 °C) at first, followed by oil-cooling after holding for a certain period of time, and then tempering at the most suitable tempering temperature (250 °C) followed by air-cooling; then, the samples were put into a deep cryogenic box with the temperature lowered to −120 °C at a rate of 5 °C/min. Different

batches of samples were held at the temperature for 1 h, 2 h, and 3 h, respectively. Finally, the samples within the deep cryogenic box returned to room temperature gradually when the cooling system was turned off. The heat treatment process is shown in Table 2.

Table 2. Experimental parameters of subsequent heat treatments.

Experimental Parameter	Values
Quenching temperature (°C)	900
Quenching time (min)	20
Tempering temperature (°C)	250
Tempering time (h)	2.5
Cryogenic temperature (°C)	−120
Cryogenic time (h)	1, 2, 3

2.3. Microstructural and Mechanical Property Analyses

Uniaxial tensile experiment was conducted with an MTS809 testing machine at room temperature, and the strain rate was 1 mm/min. Three batches of tensile experiments were carried out to reduce the test errors. The samples used in the tests were spark-cutting-machined, as shown in Figure 2. Charpy impact experiments were conducted in SCHENCK−100 KN charpy tester at room temperature, and the samples were machined into standard V-notch with the dimension of 55 × 10 × 10 mm^3 according to GB/T229-2007 [23].

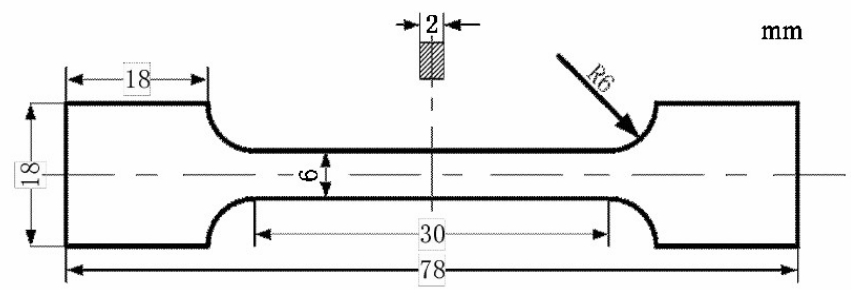

Figure 2. Diagrammatic sketch of a tensile sample at room temperature.

The microstructure and fracture morphology under different conditions were observed and analyzed by an electron backscatter diffraction (EBSD) installed in JEOL 7800 F scanning electron microscopy (SEM, Japan Electron Optics Laboratory Co., Ltd., Tokyo, Japan). The dislocation density was measured by X-ray diffractometry (XRD, Empyrean, PANalytical B.V., Almelo, The Netherlands) using a D/max-2500 pc at 50 kV and 0.02° step size. The 2θ angular interval was from 40° to 140° and step-scanned with 5 s, and the target material was copper with wavelength of λ = 0.15418 nm.

3. Results

3.1. Mechanical Properties

Figure 3 shows the true stress–strain curve obtained from the tensile test for Cr-Mn-Si-alloyed high-strength steel of different deep cryogenic times. It can be found that there was no obvious yield point and yield plateau, while the yield strength decreased but the tensile strength increased with the increase in deep cryogenic time, as shown in Figure 4. The yield strength was 404 MPa, 392 MPa, 374 MPa, and 333 MPa at the deep cryogenic time of 0 h, 1 h, 2 h, and 3 h, respectively; the stress of the sample reached the peak tensile strength at the time of necking. In contrast, the tensile strength was improved to a greater extent when the deep cryogenic time was 1 h, while the yield strength only decreased by about 10 MPa. When the deep cryogenic time was extended to 2 h and 3 h, the yield strength decreased significantly and the tensile strength increased less. Therefore, it can be determined that 1 h was a more suitable deep cryogenic treatment process parameter.

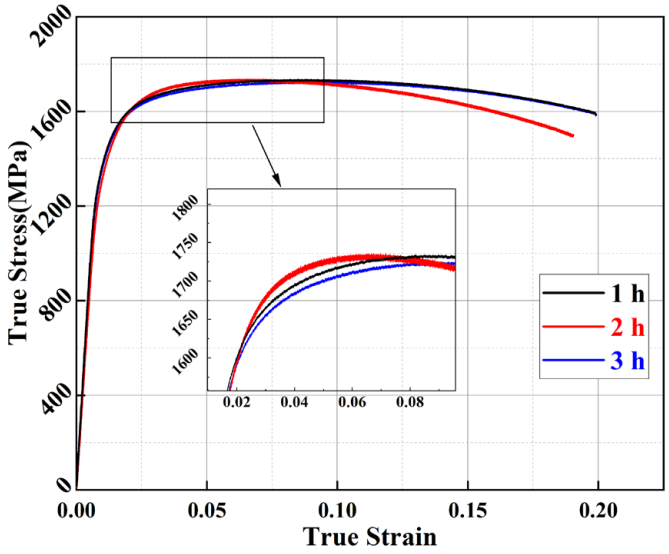

Figure 3. True stress–strain curves for Cr-Mn-Si high-strength alloyed steel at different deep cryogenic time tensioned at room temperature.

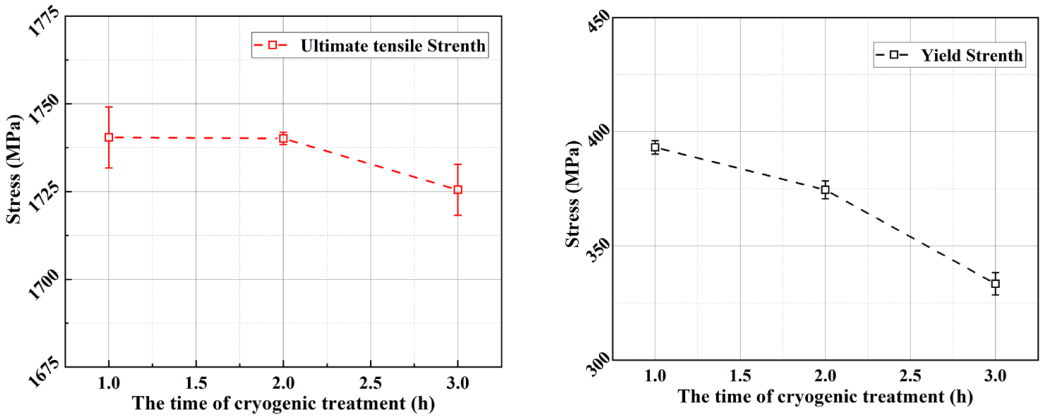

Figure 4. Variation in yield strength and tensile strength at different deep cryogenic time.

3.2. Microstructure Analyses

Due to the influence of alloying elements, the start temperature of the martensite transformation is about 314 °C and the end temperature is below room temperature. According to Meng's research [24], when the alloy steel is held in the austenite temperature zone, the carbon element starts to dissolve when the heating temperature in the austenite zone exceeds the A3 line. The austenite transforms into martensite due to rapid cooling of quenching, and then part of the martensite reverses to austenite after the tempering process, which enhances the toughness of the material. As shown in Figure 5a, the martensite microstructure in the tempered samples shows a morphology of a dense parallel slat pattern after rapid quenching, with the pristine austenite grain boundary (PAGB) acting as the boundary, and martensite slats being distributed along all directions. Residual austenite could also be found after different times of deep cryogenic treatment, as shown in Figure 5b–d. Owing to incomplete martensitic phase transformation, the residual austenite was scattered in the martensitic matrix. Moreover, in addition to slate-like martensite and residual austenite, lamellar martensite grains could also be observed after the deep cryogenic treatment of Cr-Mn-Si-alloyed high-strength steel.

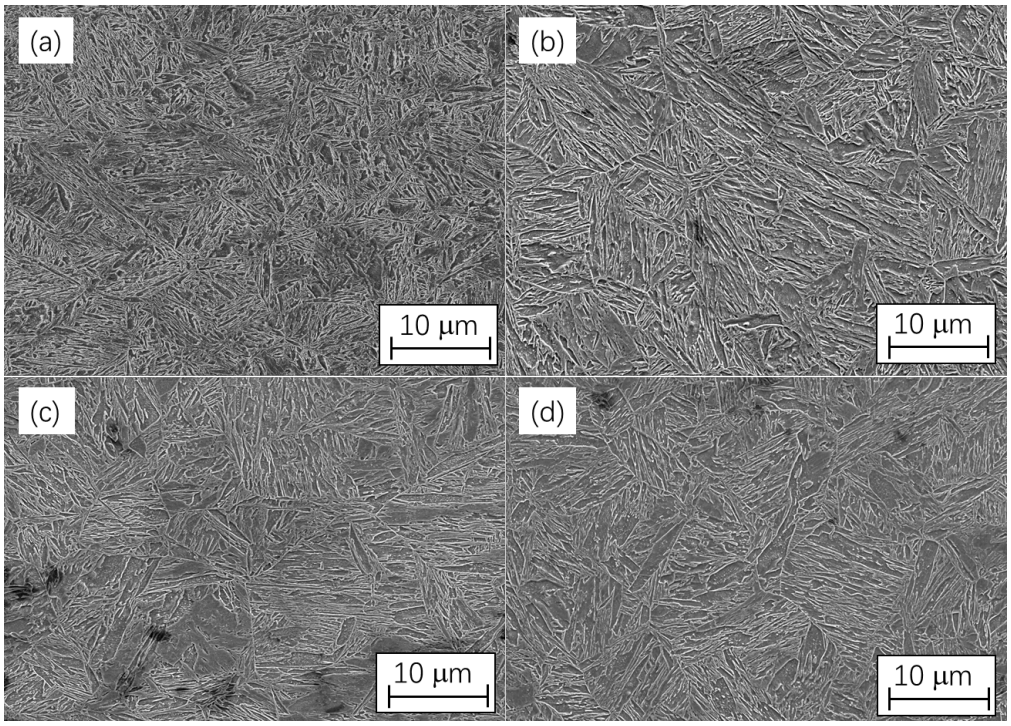

Figure 5. SEM images of Cr-Mn-Si-alloyed high-strength steel during cryogenic process at different treatment time: (**a**) 0 h, (**b**) 1 h, (**c**) 2 h, (**d**) 3 h.

As shown in Figure 5, when Cr-Mn-Si-alloyed high-strength steel was treated at different deep cryogenic time, the proportion of residual austenite reduced and the martensite laths formed by the transformation of the original austenite grains became course as the treatment time prolonged, while the lamellar martensite gradually increased when comparing to slatty martensite. Moreover, the grains were relatively fine and the average size of the secondary carbides precipitated inside the matrix were significantly reduced after the deep cryogenic treatment, and were uniformly distributed in the martensitic matrix.

The impact fracture morphologies at four different deep cryogenic times are shown in Figure 6. It can be seen that the fracture form of the quenched–tempered samples were basically microporous aggregated, as shown in Figure 6a. A large amount of micropores could be observed in the SEM images, which contributed to a better impact toughness. However, when the tempered samples were deep-cooled for a certain period of time, the cleavage steps appeared in the internal radiation stripe areas in the impact fracture gradually, and the proportion of the cleavage steps increased with the extension of the deep cryogenic time, as shown in Figure 6b–d. The cleavage steps were relatively few when the deep cryogenic time was 1 h. When the deep cryogenic time increased to 2 h, a large number of small and shallow dimples were distributed on the side of the cleavage steps, and the sample showed a quasi-deconstruction fracture. When the deep cryogenic time increased to 3 h, the impact fracture showed an obvious river pattern, in which each branch of the river pattern consisted of a bunch of parallel-arranged cleavage steps with different heights. A large number of tearing edges and many micropores were scattered inside the branch and no dimples were basically observed, which was characterized by a classical brittle fracture.

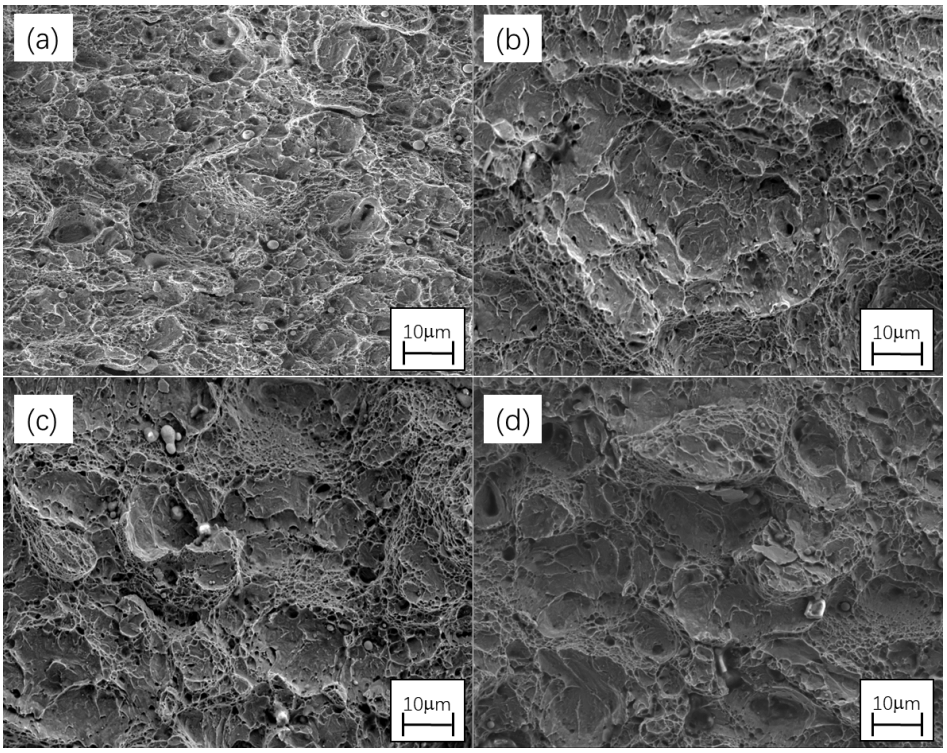

Figure 6. SEM diagram of impact fracture for different cryogenic processes. (**a**) 0 h. (**b**) 1 h. (**c**) 2 h. (**d**) 3 h.

4. Discussion

4.1. Effect of Deep Cryogenic Treatment Process on the Mechanical Properties and Microstructure of Cr-Mn-Si-Alloyed High-Strength Steel

As shown in Figure 5, more fine secondary carbides were uniformly distributed within the matrix and the average size of carbides was significantly reduced when the sample was Q-T and deep-cryogenic-treated, which is ascribed to the martensitic phase transformation of residual austenite in the low-temperature environment. The low-temperature martensitic transformation process was often accompanied by plastic deformation, and the stress generated by plastic deformation induced the dissolution of large-size carbide particles. Hence, the larger-sized carbide of the specimen produced after the Q-T process was reduced, and there was a large number of fine secondary carbide precipitation diffuse and uniformly distributed in the matrix.

Figure 7 shows the localized enlarged SEM images of the samples that were deep-cryogenic-treated for 1 h and 3 h. It can be observed that the carbon particles and residual austenite were distributed at the PAGB, and that the residual austenite was distributed in the form of a thin film when deep-cryogenic-treated for 1 h. In the process of quenching, the carbon element diffused from the martensite to the surrounding austenite, induced an increase in the carbon content, and thereafter enhanced the stability of residual austenite film, which was beneficial to the improvement in toughness for Cr-Mn-Si-alloyed high-strength steel. As shown in Figure 8, the tempered sample was accompanied by martensite lattice shrinkage and carbon precipitation during deep cryogenic treatment, which had two effects on the properties of the sample microstructure: first, the strength of the sample softened from the martensite decarburization; second, the carbon atoms precipitated in martensite had a low diffusion drive in the deep cryogenic chamber at −120 °C, and therefore precipitated in the form of carbides in the matrix and were unable to diffuse into the untransformed austenite, which gave rise to an obvious improvement in strength resulting from precipitation strengthening and fine crystal strengthening. The combination of the above-mentioned softening and strengthening effect determined the mechanical properties of the deep cryogenic sample.

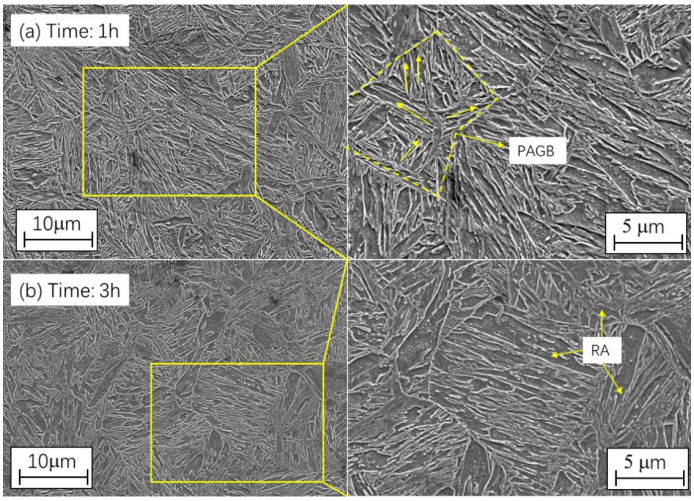

Figure 7. SEM images of Cr-Mn-Si-alloyed high-strength steel during cryogenic process at (**a**) 1 h, (**b**) 3 h. (The right image is the area marked by the yellow square in the left image.)

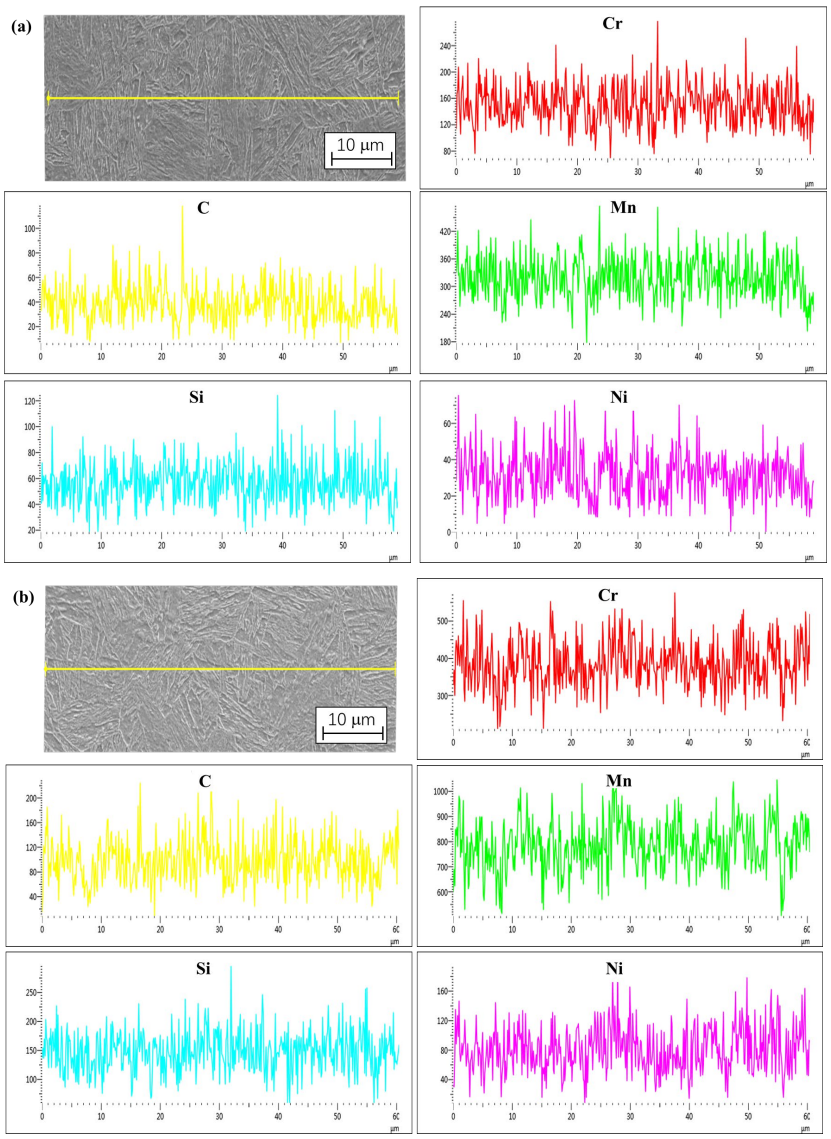

Figure 8. Results of EDS line analysis conducted on the Cr-Mn-Si-alloyed high-strength steel sample in cryogenic treatment for (**a**) 1 h and (**b**) 3 h.

As previously mentioned, during the process of deep cryogenic treatment, residual austenite in the material underwent continuous transformation into martensite, thereby enhancing its strength. Additionally, secondary carbides precipitated due to the shrinkage of the martensite lattice and elements in the matrix rearranged themselves (as shown in Figure 8a), forming a diffuse distribution of second-phase particles within the matrix that produce strengthening effects through interaction with stress fields and dislocations. Consequently, deep cryogenic samples exhibited a higher tensile strength but lower yield strength than those treated solely with Q-T methods. While residual austenite continuously transformed into martensite as the deep cryogenic time increased, this transformation was limited by temperature; it ended when the treatment time reached 2 h (as illustrated in Figure 8b). This explains why the grain size remained constant at 2 h and 3 h of deep cryogenic treatment but differed from that after 1 h.

Figure 9 shows the inverse pole figure and the average grain size of Cr-Mn-Si-alloyed high-strength steel at different deep cryogenic treatment times. It can be observed that the average grain size of the sample was much smaller when the deep cryogenic time was 1 h than that of 2 h and 3 h, which also explains the relatively better overall performance when the deep cryogenic was 1 h.

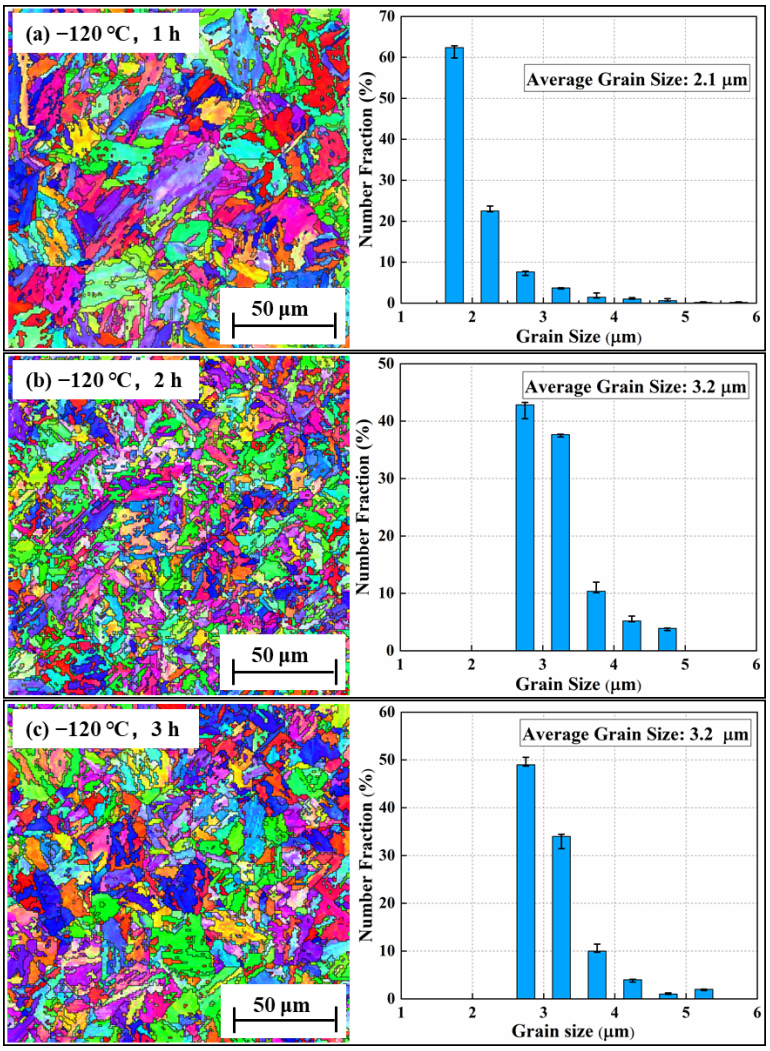

Figure 9. Microstructural changes of Cr-Mn-Si high-strength alloyed steel at different cryogenic treatment times: (**a**) 1 h, (**b**) 2 h, (**c**) 3 h.

With the growth in deep cryogenic time, the size of martensite grains gradually increased, as shown in Figure 9, decreasing the yield strength. Martensite transformation of alloy steel started at the temperature of 314 °C (Ms), and ended at the transformation

temperature of −30 °C; due to the temperature dropping below the phase transition termination temperature, the greater the subcooling degree, the greater phase transition drive force, prompting the residual austenite-to-martensite transformation. In the deep cryogenic treatment, due to the martensite lattice contraction at very low temperatures, quenched martensite decarburization occurred, and carbon atom bias polymerized in the samples. The residual austenite absorbed the carbon atoms convergence due to lattice mismatch, so its carbon content increased. As is known, the carbon content and alloying content decide the formation of lath martensite in the great degree of subcooling, and thus the new formation of the martensite in the lath martensite was relatively higher, as shown in Figure 7. It is known that lath martensite is relatively hard and brittle, while its notch sensitivity is also relatively low, so the yield strength decreased, tensile strength increased, and impact toughness decreased with the growth in deep cryogenic time.

In crystallography, the grain boundaries with an orientation angle lower than 15° are generally referred to as low-angle grain boundaries (LAGBs), and the grain boundaries with an orientation angle greater than 15° are referred to as high-angle grain boundaries (HAGBs). Figure 10 shows the orientation angle distribution of alloy steel at different deep cryogenic treatment times, and it can be seen from the figure that the increased deep cryogenic time makes the proportion of LAGBs decrease while the proportion of HAGBs increases. The reason for this phenomenon is that, under the premise that the deep cryogenic temperature is determined, as the treatment time increased, the transformation of residual austenite into martensite and the shrinkage of the original martensite lattice gradually occurred, forming new grain boundaries, and the newly formed grain boundaries tend to form dislocation plugging, resulting in an increase in the momentum required for free dislocation movement, thus making the tensile strength of the material increase. At the same time, alloying elements have relatively more time to diffuse in the matrix with the transformation of residual austenite into martensite. As shown in Figure 8, the aggregation of alloying elements on the free dislocation pegging for dislocation transformation into LAGBs and then the formation of stable HAGBs played a positive role in promoting the process [25], which can improve the tensile strength of alloyed steel.

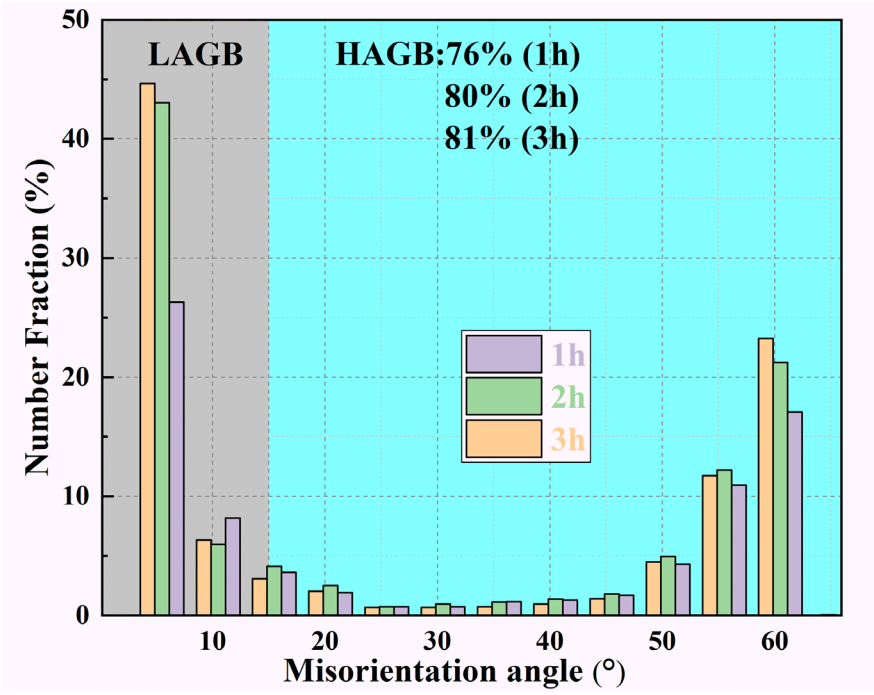

Figure 10. Orientation angle distribution of Cr-Mn-Si-alloyed high-strength steel when stretched at cryogenic treatment time.

4.2. Effect of Deep Cryogenic Treatment Process on Cr-Mn-Si High-Strength Dislocation Density

The XRD diffraction patterns of Cr-Mn-Si-alloyed high-strength steel at different deep cryogenic treatment times are shown in Figure 11a. Martensitic diffraction peaks were selected from the diffraction angle range of 40° to 140° with crystallographic lattice coefficients of (110) (200) (211) (220) (310) after different treatment times for Cr-Mn-Si-alloyed high-strength steel, which have the same diffraction peaks at the same diffraction angle, which indicates that the different deep cryogenic treatment times do not affect the lattice constants. The half-width height (FWHM) of each diffraction peak can be obtained automatically by using MDI Jade to analyze the XRD data. However, the FWHM of the same crystallographic index after different treatment times differed greatly, and the peak widths of the diffraction peaks had different degrees of broadening, as shown in the local magnification of Figure 11a.

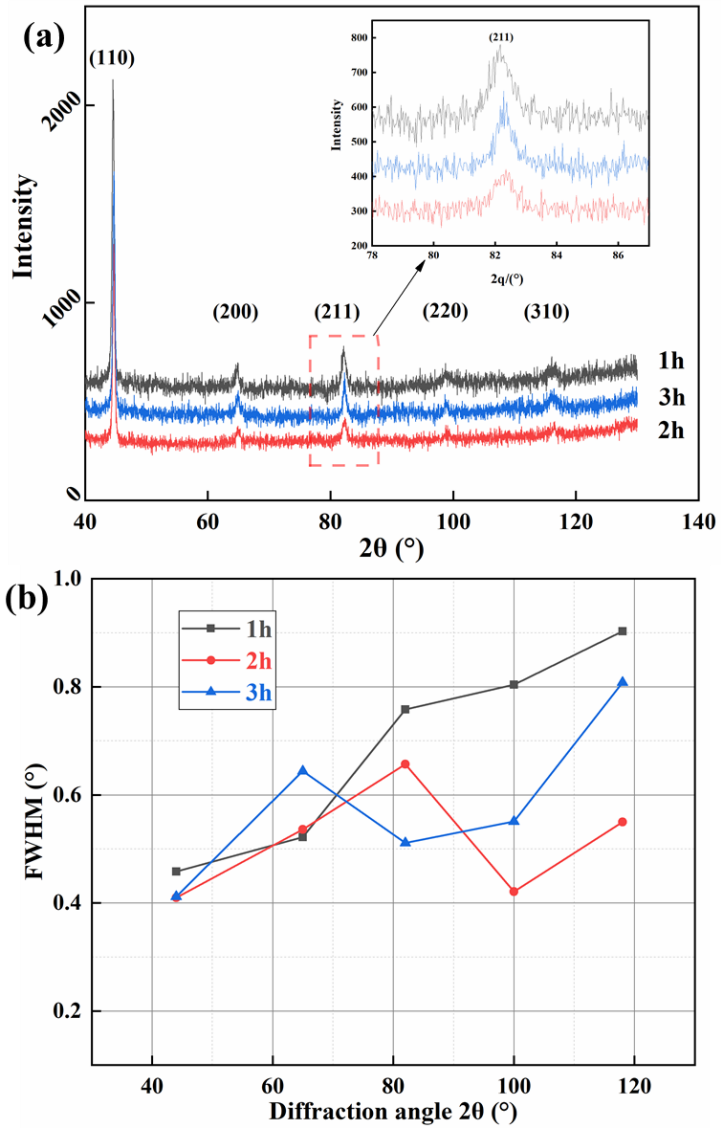

Figure 11. XRD pattern and FWHM distribution of Cr-Mn-Si-alloyed high-strength steel: (**a**) ZRD pattern, (**b**) FWHM.

The XRD-WH method, proposed by Williamson and Hall in the 1950s, suggests that diffraction peak width variations are caused by grain surface distortion, while lattice

distortion can arise due to atomic solid solution, twinning, dislocations, etc. [26], and that the diffraction peak width and strain can be shown by the following equation:

$$\delta\frac{\cos\theta}{\lambda} = \alpha + 2\varepsilon\frac{\sin\theta}{\lambda} \quad (1)$$

where $\alpha = 0.9/D$, D is the grain size (m), θ is the diffraction angle (°), λ is the wavelength of the X-rays (m, 0.15418 nm), and ε is the strain. The relationship between dislocation density and strain can be expressed by Equation (2):

$$\rho = 14.4\frac{\varepsilon^2}{b^2} \quad (2)$$

where b is the Platz vector of dislocations, and since the crystal structure of martensite is body-centered cubic (bcc), b = 0.248 nm [27]. It can be seen from the equation that the dislocation density is positively correlated with the strain, and, to facilitate the calculation of the material strain, Equation (1) can be expressed as shown in Equation (3):

$$\Delta K = \alpha + \varepsilon K \quad (3)$$

K is considered the fundamental unit of the diffraction vector, which is expressed as

$$K = \frac{2\sin\theta}{\lambda} \quad (4)$$

K can then be considered as the diffraction peak width in K, which is expressed as

$$\Delta K = \delta\frac{\cos\theta}{\lambda} \quad (5)$$

According to Equation (3), there is a linear relationship between K and K. The slope is the microstrain of the microstructure, which can be obtained by substituting the FWHM value into the equation. The least squares method can be used for linear fitting, and then can be substituted into Equation (2) to find the value of dislocation density, as shown in Figure 12.

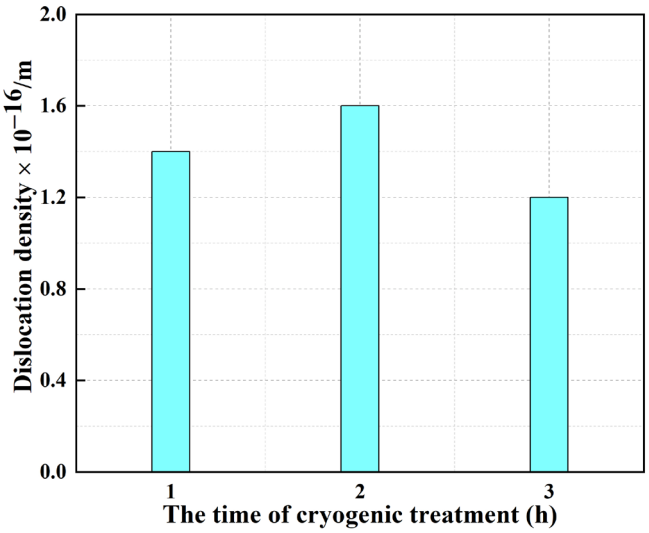

Figure 12. The dislocation density of Cr-Mn-Si-alloyed high-strength steel based on XRD analysis.

From the analysis of XRD results, it can be seen that the dislocation density of Cr-Mn-Si-alloyed high-strength steel was greatly affected by the deep cryogenic treatment, where the dislocation density of the alloy steel increased significantly compared with that of the

Q-T samples, having the highest dislocation density at 2 h of the deep cryogenic process (rising by about 30%), but decreased by 25% when the time extended to 3 h. This proves the argument that the transformation of residual austenite into martensite at a 2 h deep cryogenic time was over. The possible reason for the longer deep cryogenic time taken to reduce the dislocation density in the matrix could be due to the stabilization of the matrix microstructure with the prolonged low-temperature time, and the release of residual stress in the microstructure and the disappearance of part of the dislocation structure. On the one hand, the higher dislocation density played a role in dislocation strengthening; on the other hand, more vacancies and diffusion channels were provided for the diffusion of matrix elements, which theoretically explains the phenomenon shown in Figure 8.

5. Conclusions

(1) For Cr-Mn-Si-alloyed high-strength steel, deep cryogenic treatment after Q-T treatment improved the microstructure and mechanical property of the material. The better deep cryogenic process parameter was −120 °C + 1 h after the Q-T process.
(2) The microstructure of Cr-Mn-Si-alloyed high-strength steel after deep cryogenic treatment was tempered martensite and diffusely distributed carbides, which refined the matrix microstructure and made the martensite slats more uniform. However, with the extension of deep cryogenic time, lath martensite gradually appeared.
(3) The dislocation density of Cr-Mn-Si-alloyed high-strength steel was influenced by the deep cryogenic treatment, and was highest at a deep cryogenic treatment time of 2 h.

Author Contributions: Conceptualization, J.Z. and Y.M.; methodology, J.Z.; software, H.M.; validation, R.S.; formal analysis, J.F.; investigation, J.Z.; data curation, H.M.; writing—original draft preparation, J.Z.; writing—review and editing, Y.M.; visualization, J.Z.; supervision, Y.M. All authors have read and agreed to the published version of the manuscript.

Funding: This research received no external funding.

Data Availability Statement: Data availability does not apply to this article as no new data were created or analyzed in this study.

Conflicts of Interest: The authors declare no conflict of interest.

References

1. Chen, Z.Z.; Lan, D.N.; Ma, D.S. *Die Steel Manual*; Metallurgical Industry Press: Beijing, China, 2020; Volume 4, pp. 326–328.
2. Wang, H.J.; Zhang, Y.H.; Li, Y.Y.; Long, J.; Ma, Z.X. Low Cycle Fatigue Properties of Electron Beam Welding Joint of 30CrMnSiNi2A Ultra-High Strength Steel. *Hot Work. Technol.* **2022**, *51*, 58–62.
3. Pang, J.L.; Zhu, Z.L.; Zhang, J.Y.; Chen, Q.; Zhou, J.; Meng, Y.; Sugiyama, S. Thermal forming properties of a Cr-Mn-Si-Ni alloyed naval steel under different forming conditions by different constitutive models. *Rare Met.* **2021**, *41*, 3515–3529. [CrossRef]
4. Duan, Y.T.; Zhu, W.T.; Liu, W.S.; Ma, Y.Z.; Cai, Q.S.; Cai, Y. A novel strategy for preparing high-performance powder metallurgical low alloy ultrahigh strength steel. *Mater. Sci. Eng. A* **2023**, *864*, 144585. [CrossRef]
5. Li, J.H.; Zhan, D.P.; Jiang, Z.H.; Zhang, H.S.; Yang, Y.K.; Zhang, Y.P. Progress on improving strength-toughness of ultra-high strength martensitic steels for aerospace applications, a review. *J. Mater. Res. Technol.* **2023**, *23*, 172–190. [CrossRef]
6. Duan, Y.T.; Liu, W.S.; Ma, Y.Z.; Cai, Q.S.; Zhu, W.T.; Liu, J. Effect of Ni addition upon microstructure and mechanical properties of hot isostatic pressed 30CrMnSiNi2A ultrahigh strength steel. *Mater. Sci. Eng. A* **2022**, *850*, 143599. [CrossRef]
7. Dwivedi, P.K.; Vinjamuri, R.; Rai, A.K.; Ganesh, P.; Ranganathan, K.; Bindra, K.S.; Dutta, K. Effect of laser shock peening on ratcheting strain accumulation, fatigue life and bulk texture evolution in HSLA steel. *Int. J. Fatigue* **2022**, *163*, 107033. [CrossRef]
8. Yuan, S.Q.; Shen, Z.X.; Zhou, C.H.; Liu, F.T.; Wang, F.; Yang, H.; Chen, J. Study on Mechanical Properties of 30CrMnSiNi2A Steel under Simulated Alternating High and Low Air Conditions. *Mater. Sci. Technol.* **2015**, *23*, 125–128.
9. Zhou, Y.Q.; Zhang, Y.M. Effect of Heat Treatment on Microstructure and Dynamic Properties of 30CrMnSiNi2A Steel. *Forg. Equip. Manuf. Technol.* **2010**, *45*, 80–83.
10. Widiantara, I.P.; Machendradhany, A.P.; Putra, D.P.; Yang, H.W.; Park, K.S.; Ko, Y.G. Achieving high fracture toughness and tribological properties in high-carbon steels via sub-zero treatment and low-temperature tempering. *J. Alloys Compd.* **2020**, *821*, 153195.
11. Yan, X.G.; Li, D.Y. Effects of the sub-zero treatment condition on microstructure mechanical behavior and wear resistance of W9Mo3Cr4V high speed steel. *Wear* **2013**, *302*, 854–862. [CrossRef]

12. Sobotova, J.; Jurci, P.; Dlouhy, I. The effect of subzero treatment on microstructure, fracture toughness, and wear resistance of Vanadis 6 tool steel. *Mater. Sci. Eng. A* **2016**, *625*, 192–204. [CrossRef]
13. Yang, J.; Zhang, W.D.; Zheng, K.D.; Dang, J.Z.; Xu, H. Effect of deep cryogenie treatment time on microstrueture and tensile strength of A319 alloy. *Trans. Mater. Heat Treat.* **2014**, *35*, 181–184.
14. Liu, Y.; Liu, X.L.; Zhang, J.D. Effect of cryogenic treatment on mechanical properties of Cr12MoV steel. *Heat Treat. Met.* **2011**, *36*, 3840.
15. Hu, H.B.; Zhu, L.H.; Tu, Y.W.; Duan, Y.M.; Wu, X.C.; Gu, B.F. Effect of Cryogenic Treatment on Microstructure and Properties of M2 High Speed Steel. *Mater. Rep.* **2023**, *37*, 171–176.
16. Wang, J.B.; Sun, X.Y.; Su, B.Y.; Zhang, S. Effect of Cryogenic treatment Times on wear and Corrosion Resistance of E690 Steel. *Hot Work. Technol.* **2022**, *51*, 147–151.
17. Li, H.; Yi, T.T.; Liu, Y. Effect of Cryogenic Treatment on Properties of GCr15 Bearing Steel. *Bearing* **2015**, *8*, 41–44.
18. Zhao, X.L.; Luo, X.Y.; Yu, L.D.; Wang, Y.J.; Jia, Z. Effect of Cryogenic Treatment on Microstructure and Mechanical Properties of Inconel617 Alloy. *J. Lanzhou Univ. Technol.* **2023**, *49*, 7–11.
19. Jurci, P.; Bartkowska, A.; Hudakova, M.; Domankova, M.; Caplovicova, M.; Bartkowski, D. Effect of Sub-Zero Treatments and Tempering on Corrosion Behaviour of Vanadis6 Tool Steel. *Materials* **2021**, *14*, 3759. [CrossRef] [PubMed]
20. Perez, M.; Belzunce, F.J. The effect of deep cryogenic treatments on the mechanical properties of an AISI H13 steel. *Mater. Sci. Eng. A* **2015**, *624*, 32–40.
21. Dhokey, N.B.; Maske, S.S.; Ghosh, P. Effect of tempering and cryogenic treatment on wear and mechanical properties of hot work tool steel (H13). *Mater. Today Proc.* **2021**, *43*, 3006–3013. [CrossRef]
22. Chen, Y.Q.; Wu, Y.W.; Qin, Z.W.; Zhou, X.; Wang, H.B. Effects of deep cryogenic treatment on microstructure and mechanical properties of GCr15 bearing steel. *Mater. Mech. Eng.* **2018**, *42*, 55–58. [CrossRef]
23. Zong, Q.L.; Sun, H.; Wang, H.Y.; Cui, E.W. Metallic materials-Charpy pendulum impact test method. *Phys. Test. Chem. Anal. Part B Chem. Anal.* **2010**, *3*, 190–192.
24. Meng, Y.; Sugiyama, S.; Soltanpour, M.; Yanagimoto, J. Effects of predeformation and semisolid processing on microstructure and mechanical properties of Cr-V-Mo steel. *J. Mater. Process. Technol.* **2013**, *213*, 426–433. [CrossRef]
25. Zhang, J.Y.; Jiang, P.; Zhu, Z.L.; Chen, Q.; Zhou, J.; Meng, Y. Tensile properties and strain hardening mechanism of Cr-Mn-Si-Ni alloyed ultra-strength steel at different temperatures and strain rates. *J. Alloys Compd.* **2020**, *842*, 15586. [CrossRef]
26. Williamson, G.K.; Smallman, R.E. Dislocation densities in some annealed and cold-worked metals from measurements on the X-ray Debye-Scherrer spectrum. *Philos. Mag.* **1955**, *1*, 34–46. [CrossRef]
27. Cui, J.; Liu, Y.Z.; Pan, H.; Gao, L.F. Reheating Austenitizing Temperature of Spring Steel 60Si2MnA for Railway. *J. Iron Steel Res. Int.* **2008**, *15*, 62–67. [CrossRef]